Significant Findings Statement

"Surface Soil Moisture Retrieval Using SSM/I and Its Comparison with ESTAR: A Case Study over a Grassland Region"

T. Jackson, A. Hsu, and P. O'Neill

Question: Previous studies by some researchers suggest that microwave data with frequencies higher than 10 GHz are not appropriate for soil moisture estimation since the vegetation will strongly mask out most surface information at these high frequencies. However, in a recent study, Calvet et al. indicated that the top surface soil moisture can be retrieved with acceptable accuracy at higher microwave frequencies with a theoretical model if vegetation coverage is less than 50% of the area or if vegetation such as agricultural crops are at an early stage of growth. This study addresses whether 19 GHz SSM/I data over a grassland region can be used to retrieve surface soil moisture accurately.

Approach: A semi-empirical algorithm developed by Jackson was applied to 19 GHz SSM/I data along with other ancillary data such as NDVI derived from AVHRR and effective temperature derived from Oklahoma MESONET measurements. In addition, a Geographic Information System (GIS) approach was adapted to organize required parameters into a database format to facilitate the evaluation of SSM/I data for surface soil moisture retrieval. The surface soil moisture values retrieved using this algorithm were compared both to ground measurements of soil moisture and to soil moisture estimated with L band microwave data from the Electronically Scanned Thinned Array Radiometer (ESTAR) using the same retrieval algorithm. These comparisons were made using data sets collected as part of the Southern Great Plains 1997 (SGP97) Hydrology Experiment in Oklahoma over three intensive sampling areas of different vegetation regimes.

Significance: Results indicate that a soil moisture retrieval accuracy of 7.81% could be achieved with SSM/I data as contrasted to 2.82% with the L band ESTAR data. A comparison of surface soil moisture images derived from SSM/I and from ESTAR shows that SSM/I soil moisture images retain the regional wet/dry pattern, but lose the local details that can be found in ESTAR moisture images. These results confirm that under certain conditions SSM/I data can be used to retrieve surface soil moisture information at a regional scale. These results are of value in the development of future satellite instruments as well as for extracting useful information for hydrology and agriculture from the current SSM/I instruments in orbit.

Relation to Earth Science Enterprise science plan: Land surface variability and water process studies (soil moisture)

Surface Soil Moisture Retrieval Using SSM/I and Its Comparison with ESTAR: A Case Study over a Grassland Region

T.J. Jackson
USDA-ARS Hydrology Lab, 104 Bldg 007, BARC-West, Beltsville, MD 20705

A.Y. Hsu
SSAI, USDA-ARS Hydrology Lab, 104 Bldg 007, BARC-West, Beltsville, MD 20705

P.E. O'Neill
Hydrological Sciences Branch/974, Laboratory for Hydrospheric Processes,
NASA/Goddard Space Flight Center, Greenbelt, MD 20771

Abstract. This study extends a previous investigation on estimating surface soil moisture using the Special Sensor Microwave/Imager (SSM/I) over a grassland region. Although SSM/I is not optimal for soil moisture retrieval, it can under some conditions provide information. Rigorous analyses over land have been difficult due to the lack of good validation data sets. A scientific objective of the Southern Great Plains 1997 (SGP97) Hydrology Experiment was to investigate whether the retrieval algorithms for surface soil moisture developed at higher spatial resolution using truck- and aircraft-based passive microwave sensors can be extended to the coarser resolutions expected from satellite platform. With the data collected for the SGP97, the objective of this study is to compare the surface soil moisture estimated from the SSM/I data with those retrieved from the L-band Electronically Scanned Thinned Array Radiometer (ESTAR) data, the core sensor for the experiment, using the same retrieval algorithm. The results indicated that an error of estimate of 7.81% could be achieved with SSM/I data as contrasted to 2.82% with ESTAR data over three intensive sampling areas of different vegetation regimes. It confirms the results of previous study that SSM/I data can be used to retrieve surface soil moisture information at a regional scale under certain conditions.

1. Introduction

This study extends a previous investigation on estimating surface soil moisture using the Special Sensor Microwave/Imager (SSM/I) over a grassland region. In the earlier study, Jackson (1997) applied a physically based model to relate satellite data to ground observations based on sampling sites distributed over the study area. Vegetation water content measured at these sites was used to correct for the vegetation attenuation effect on the microwave signal. He concluded that over the Little Washita watershed, a grass dominated subhumid area, a soil moisture-emissivity relationship could be developed to incorporate the range of temperature and vegetation conditions encountered with an error of estimate of 5.3%. It was also pointed out that further study was needed for adapting this approach to other vegetation regimes. In this study, data collected for the Southern Great Plains 1997 (SGP97) Hydrology Experiment were used to verify and to extend Jackson (1997) since SGP97 consisted of three intensive sampling areas with different vegetation regimes.

In Jackson (1997), a procedure developed by Choudhury (1993) was used to correct for atmospheric attenuation on SSM/I data. This procedure estimated the atmospheric transmission coefficient at the frequencies of 19 and 37 GHz as a function of the average precipitable water vapor, a variable which can be readily obtained from published climate data records. For the current study, atmospheric scattering, absorption and emission behavior were computed from atmospheric profiles measured by balloon-borne sounding systems during SGP97.

Vegetation effects on the microwave radiometric sensitivity to soil moisture have been studied by various researchers (i.e., Kirdiashev et al., 1979, Jackson et al., 1982, Ulaby et al., 1983, Jackson and Schmugge, 1991, Ferrazzol et al., 1992, and Calvet et al., 1995b).

Many of these studies have been based on the data collected by truck mounted radiometers over a single specific type of vegetation (Jackson et al., 1982, Pampaloni and Paloscia, 1986, Paloscia and Pampaloni, 1992, and Calvet et al., 1995b). However, more than one type of vegetation will often be found in a satellite footprint. It is difficult to apply theoretical vegetation models (Calvet et al., 1995b) that require many parameters to account for the vegetation contribution to the microwave emission from the earth's surface. The semi-empirical approach (Jackson et al., 1982, and Jackson and Schmugge, 1991) can be easier to implement because it requires fewer parameters. Even with this approach, however, it is still necessary to make some modification of the parameters in order to adapt the results of these previous studies for correcting for vegetation effects on satellite microwave data. SGP97 also offered data from an L-band radiometer which provided an opportunity to evaluate the reduction of sensitivity in soil moisture retrieval due to the SSM/I's higher frequencies.

2. Southern Great Plains 1997 Hydrology Experiment

The SGP97 was an interdisciplinary science hydrology experiment which included the objective of validating that the retrieval algorithms for surface soil moisture developed at higher spatial resolution using track- and aircraft-based sensors can be extended to the coarser resolutions expected from satellite platforms (Jackson et al., 1999). Surface soil moisture was mapped over an 10,000 km^2 area at an 800 m resolution with the L band Electronically Scanned Thinned Array Radiometer (ESTAR) on a daily basis for a month. The experiment took place from June 18 to July 17, 1997 in Oklahoma. The area coverage ranged from the Little Washita River watershed in the south to the Department of Energy's Central Facility for the Atmospheric Radiation Measurement (ARM)

program near the Kansas border in the north. Extensive ground measurements of soil moisture were collected at the Little Washita watershed (LW), the Central Facility area (CF), and USDA's research laboratory at El Reno (ER) west of Oklahoma City (Figure 1).

The Little Washita watershed, covers an area of 603 km^2, is instrumented with USDA/ARS Micronet for hydrologic research. Soils include a wide range of textures with large regions of both coarse and fine textures. Land use is dominated by rangeland and pasture (63%) with significant areas of winter wheat and other crops concentrated in the floodplain and western portions of the watershed area. The Grazinglands Research Laboratory at El Reno, operated by USDA ARS, consists of 24.3 km^2 of government operated grasslands. Generally, this area is a mixture of grasslands and winter wheat. However, most of the grasslands in the El Reno area are ungrazed and have significantly greater biomass than the other two intensive measurement areas. The area surrounding the DOE ARM Central Facility site is dominated by winter wheat which was ready for harvest or was harvested (wheat stubble) at the start of SGP97.

With the verification of the ESTAR soil moisture retrieval algorithm as a primary consideration, soil moisture sampling of the 0-5 cm layer was carried out in fields approximately a quarter section (0.8 km by 0.8 km) in size. Attempts were made to sample several adjacent fields that could be clustered to facilitate comparison with remotely sensed microwave measurements. The sampling performed in these fields involved two transects separated by 400 m with a sample every 100 m resulting in 14 samples per field. In addition, other smaller sites were also sampled. In total, there were 10 sites sampled in the LW, 15 in the ER, and seven in the CF. The results for each field

in a particular area were averaged together to compute a single average soil moisture value for that area on a given day. Table 1 summarizes the average volumetric soil moisture measured for the three intensive sampling areas during SGP97.

In addition to soil moisture sampling at the CF, the LW, and ER, extensive measurements of vegetation in grass/pasture and wheat fields located in these three areas were also performed during the period of June 24 to July 5 (Hollinger and Daughtry, 1999). The measurements included green and brown standing biomass, surface residue biomass, and leaf area index. In total, 48 fields were sampled, including 23 fields in the LW, 15 fields in the ER, and nine fields in the CF. More than half of these 48 fields sampled are grass/pasture. The average value of the vegetation water content over the sampled fields was about 0.373 kg/m^2 for the CF, about 0.426 kg/m^2 for the LW, and about 0.592 kg/m^2 for ER.

One of the reasons that the Southern Great Plains was selected for interdisciplinary science experiment is that it is exceptionally well instrumented for surface soil moisture, hydrology, and meteorology research. Data from two sets of instrument networks are important to this study, meteorological data from the Oklahoma Mesonet and radiosonde observations from ARM/CART. The Oklahoma Mesonet consists of 114 automated stations covering the entire state. At each station, the local environment is measured by a set of instruments located on or near a 10-meter-tall tower. Every station measures a set of seven "core parameters": air temperature and relative humidity measured at 1.5 m above the ground, wind speed and direction measured at 10 m above the ground, barometric pressure, rainfall, incoming solar radiation, and soil temperatures at 10 cm below the ground under both the natural sod cover and bare soil.

The U.S. Southern Great Plains Cloud and Radiation Testbed (CART) site was established by DOE's ARM Program. The site consists of in situ and remote-sensing instrument clusters arrayed across north-central Oklahoma and south-central Kansas. Within the ARM/CART, routine radiosonde launches take place at the Central Facility and four boundary facilities (Figure 1). The routine schedule at the CF was 0600, 1200, 1500, 1800, 2100 GMT, and at the boundary facilities only at 1800 GMT (i.e., at the local noon). During SGP97, under the so-called intensive observation period, CF and all boundary facilities had launches beginning at 230 GMT and then every three hours until 2330 GMT.

3. Microwave Instrument Description

The SSM/I is a conical scanning total power microwave radiometer system operating at a look angle of 53° and in four frequencies, 19.4, 22.2, 37, and 85.5 GHz. The 22.2 GHz channel operates in V polarization and the other three channels in both V and H polarization. The spatial resolution ranges from 69 km by 43 km at 19.4 GHz to 15 km by 13 km at 85.5 GHz. The orbital period is about 102 minutes, which results in 14.1 orbits per day. For a given satellite, coverage is possible twice a day approximately 12 hours apart on the ascending and descending passes. Additional information can be found in Hollinger et al. (1990).

Although the SSM/I was not designed for soil moisture retrieval (Heymsfield and Fulton, 1992), it is possible to extract soil moisture information under some conditions. Between June 1 and July 30, 1997, there were 179 SSM/I satellite passes that included coverage of the SGP study region from the Defense Meteorological Satellite Program (DMSP) F10, F13 and F14 platforms. These data were transferred from the

NOAA/National Environmental Satellite Data and Information Service (NESDIS) as antenna temperature. Latitude/longitude coordinates for each pixel are included with these records. These data sets were processed to reduce the data set size by eliminating scans without coverage in the SGP region and to convert the antenna temperatures to brightness temperatures. The SSM/I data were then interpolated to a standard 800 m grid to facilitate temporal analyses and comparison with the ESTAR data. The boundary of this common study region ranges from 34° N to 38.5° N and from 98.5° W to 96.6° W, or from 543,600 E to 708,400 E and from 3,764,200 N to 4,261,000 N in UTM 14S with Clarke 1886 datum. With an 800 m resolution, this common study region comprises an image with 206 pixels x 621 lines.

ESTAR is a synthetic aperture microwave radiometer operating at a center frequency of 1.413 GHz (Le Vine et al., 1994). For the SGP97 experiment, it was installed on a P-3B aircraft flown at a nominal altitude of 7.5 km to provide horizontally polarized data. With this configuration, the ESTAR data have a nominal footprint size of 400 m and were interpolated to the standard 800 m grid in the region mentioned above for all further analysis (Jackson et al., 1999). During SGP97, a total of 18 complete missions and three partial missions (truncated due to occurrence of severe weather) were successfully flown. Among these 18 complete missions, 10 were selected for this study because of proper performance of ESTAR and the removal of radio frequency interference (RFI) over the El Reno area. The CDT morning overpass of the SSM/I data taken at about the same day as the ESTAR were also selected for retrieving surface soil moisture and for the comparison with the L band data. Table 2 lists the data sets used in this study.

Figure 2 shows the brightness temperature images produced by ESTAR and SSM/I on July 2, 1997. One can observe spatial structure that corresponds to a rainfall event in the northern part of the SGP study region in both images. The major difference found between these two images is that the dynamic range in brightness temperature related to differences between wet and dry soil is much larger in the 1.4 GHz H ESTAR data than in the 19 GHz H SSM/I data.

4. Atmospheric Correction

The brightness temperature measured by the SSM/I sensors in space consists of four components:

$$T_{Bs} = T_{B1} + T_{B2} + T_{B3} + T_{B4} \tag{1}$$

where T_{B1} is the surface contribution which is the surface temperature (T_0) multiplied by the surface emissivity (e) and attenuated by the atmospheric transmissivity (t);

$$T_{B1} = T_0 * e * t \tag{2}$$

T_{B2} is the reflected downwelling atmospheric contribution (T_{dn});

$$T_{B2} = (1-e) * t * T_{dn} \tag{3}$$

T_{B3} is the extraterrestrial background contribution (T_{EX});

$$T_{B3} = (1-e) * T_{EX} * t^2 \tag{4}$$

and T_{B4} is the direct (upward) atmospheric contribution (T_{up}) and its quantity specified as being the same as T_{dn} (downwelling).

$$T_{B4} = T_{up} \tag{5}$$

In order to derive the observed surface emissivity from spaceborne microwave sensor measurements, t and T_{up} (T_{dn}) must be estimated first. The transmissivity is a function of the optical depth which is the integral of the atmospheric absorption coefficient profile.

At lower frequencies the atmospheric absorption coefficient (α), in unit of dB/km, is primarily due to atmospheric water vapor and oxygen. Following the summary provided in Ulaby et al. (1981) and Meeks and Lilley (1963), α is calculated as follows:

$$\alpha = \alpha_{H_2O} + \alpha_{O_2} \tag{6}$$

where α_{H_2O} and α_{O_2} are absorption coefficients for water vapor and oxygen, respectively. All these absorption coefficients are in unit of dB/km.

The water vapor coefficient at frequencies below 100 GHz is

$$\begin{aligned}\alpha_{H_2O} &= 2 * f^2 * \rho_v * (300/T)^{2.5} * \exp(-644/T) \\ &* (\gamma_l / ((494.4 - f^2)^2 + 4 * f^2 * \gamma_l^2)) \\ &+ 2.4 * 10^{-6} * f^2 * \rho_v * (300/T)^{1.5} * \gamma_l\end{aligned} \tag{7}$$

where f is frequency in GHz, T is temperature in K, ρ_v is the water vapor density in g/m^3, and γ_l is line width parameter in GHz

$$\gamma_l = 2.85 * (P/1013) * (300/T)^{0.626} * (1 + 0.018 * \rho_v * T/P) \tag{8}$$

where P is atmospheric pressure in mbar.

The oxygen parameter is based on the following equation which is valid for frequencies less than 45 GHz.

$$\begin{aligned}\alpha_{O_2} &= 0.011 * f^2 * (P/1013) * (300/T)^2 * \gamma * ((1/((f-60)^2 + \gamma^2)) \\ &+ (1/(f^2 + \gamma^2)))\end{aligned} \tag{9}$$

where γ is a line width parameter in GHz

$$\gamma = \gamma_0 * (P/1013) * (300/T)^{0.85} \tag{10}$$

and

$$\gamma_0 = 0.59 \qquad P \geq 333 mbar$$

$$\gamma_0 = 0.59 * (1 + 0.0031 * (333 - P)) \quad 25 \le P \le 333 mbar$$

$$\gamma_0 = 1.18 \quad P \le 25 mbar \quad (11)$$

These functions utilize the temperature, atmospheric pressure and water vapor density of an atmospheric layer. The best source to obtain these parameters is radiosonde observations collected at the exact time and place needed. For this study, the radiosonde observations were provided by the DOE's ARM/CART program. Atmospheric profiles derived from balloon soundings at the CF and one boundary facility, B6 (Figure 1), during the period of SGP97 were obtained from the ARM archive. The three variables, the air temperature, atmospheric pressure and water vapor density, required to compute the absorption coefficients were extracted from these radiosonde profiles. The atmospheric transmissivity was computed with equations 6 - 11. The value of T_{up} (T_{dn}) was integrated based on the atmospheric temperature profiles. Values of transmissivity and T_{up} (T_{dn}) for the CF and B6 were averaged to represent the atmospheric condition for the entire SGP region.

5. SSM/I Analyses and Results

To evaluate the capability of SSM/I data for surface soil moisture retrieval, a Geographic Information System (GIS) type approach was adapted. Although there were 179 SSM/I data takes obtained during SGP97, only ten were selected for this study because of the availability of ESTAR data for comparison. A database was built for each SSM/I data set listed in Table 2. The database included information for deriving surface effective temperature, vegetation attenuation, and surface roughness.

5.1. Emissivity and Volumetric Soil Moisture

After computing atmospheric transmissivity and T_{up} (T_{dn}), the surface effective temperature is the only unknown in equations 1 - 5 needed to compute the observed emissivity or normalized brightness temperature. The surface effective temperature can be approximated by a combination of the near surface air temperature and soil temperature at depth as suggested by Choudhury et al. (1982). The air temperature at 1.5 m and soil temperature at 10 cm below the surface were available from the Oklahoma Mesonet stations every fifteen minutes. The Mesonet observations that are closest in time to the SSM/I data were interpolated to the standard 800 m grid using the same software that generated the SSM/I and ESTAR data sets. Effective temperatures for the SGP area were computed and added to the GIS databases. Equations 1 - 5 were used to compute the normalized brightness temperature for each pixel. The average values of the observed emissivity for the LW were extracted from every SSM/I data set studied and are plotted against volumetric soil moisture along with results from Washita'92 and Washita'94 (Jackson, 1997) in Figure 3. The solid and dash lines in this figure are the predicted values from a theoretical model. Instead of using radiosonde data for computing atmospheric effects for the Washita'92 and Washita'94 SSM/I data, Jackson (1997) applied the empirical procedure developed by Choudhury (1993) for atmospheric correction. According to Choudhury, the magnitude of the effect of the atmosphere at midlatitudes in the summer at 19 GHz is on the order of 3° K. In Figure 3, the emissivity values derived from SSM/I data by these two atmospheric correction methods for the Little Washita watershed fall at locations close to each other and follow the trend predicted by the theoretical model. From Figure 3, one can conclude that this empirical approach provides a reasonable approximation of the atmospheric correction for SSM/I

19 GHz data. It also indicates that the physically based model described by Jackson (1997) can be used to analyze SGP97 SSM/I data.

5.2. Soil Moisture Retrieval Algorithm and Its Application to SGP97 SSM/I data

The soil moisture retrieval algorithm is well documented by Jackson (1993) and Jackson et al. (1995). When this algorithm was applied to the SGP97 SSM/I data, the step of checking land cover type was omitted since the spatial resolution of SSM/I 19 GHz data is 69 km by 43 km which includes more than one land cover type in the footprint although the data were interpolated to 800 m pixels in the database. After obtaining the soil dielectric constant by inverting the Fresnel equations, the dielectric mixing model developed by Hallikainen et al. (1985) was used to convert the soil dielectric constant to volumetric soil moisture. This is another modification of Jackson's original algorithm. The reason to select Hallikainen's mixing model instead of using Wang and Schmugge (1980) is Wang and Schmugge developed their model using only L and C band data. Although Calvet et al. (1995a) had calibrated the Wang and Schmugge mixing model for higher frequencies, their corrections are only for silt loam soils. The most challenging step in applying the algorithm is to correct for the vegetation effects using the Jackson and Schmugge (1991) approach.

The approach described by Jackson and Schmugge requires vegetation water content and a vegetation parameter b to estimate the optical depth of the vegetation layer. Although vegetation water content was sampled in some fields distributed over the three intensive sampling areas, with the SSM/I geolocation accuracy of 13 km, it is difficult to correctly locate the sampled fields in the SSM/I image. In addition, the vegetation water content data represented a snapshot of vegetation conditions between June 24 and July 5.

During SGP97 a number of discrete soil moisture drydown cycles had been observed which might have been mismatched in time with the vegetation water content actually measured in any given test field. Because of this, it was decided to use measurements from another satellite taken during SGP97 so that a hopefully more accurate average value of vegetation water content could be derived for each SSM/I pixel.

NDVI data derived from AVHRR produced by the GIMMS (Global Inventory, Modeling and Monitoring System) group at NASA/Goddard Space Flight Center were used to represent vegetation conditions. This system creates 10-day, 15-day or monthly maximum value NDVI composites at a resolution of 8 km. For this study, the NDVI data were composted into two time frames, from June 18 to June 30 and from July 1 to July 18. As shown in Figure 4, the maximum NDVI values increased overall from late June to early July. The blue boxes in the figure indicate the region of the SGP97 experiment. The maximum NDVI values along with latitude and longitude of the experiment region were extracted from the original GIMMS data and were interpolated to 800 m resolution to be imported to the database used in this study for the estimation of surface soil moisture from SSM/I data. With all of the parameters specified, the soil moisture retrieval algorithm can be applied as summarized in Figure 5. The required information for the surface roughness correction was taken from Jackson et al. (1999).

A parameter similar to the b vegetation parameter described in (Jackson et al., 1982 and Jackson and Schmugge, 1991) is needed in order to use NDVI values to estimate the optical depth of the vegetation layer. However, the b parameter as well as others such as that developed by Pampaloni and Paloscia (1986), was developed for a specific type of

vegetation. For application to large footprints, a parameter that represents a mix of various type of vegetation is needed.

A few microwave vegetation indices can be found in the literature (Paloscia and Pampaloni, 1984 and 1992) for measuring biomass and vegetation water content for agricultural crops. Three of these indices, the normalized temperature difference between 37 GHz V and 37 GHz H, the normalized temperature difference between 37 Ghz H and 19 GHz H, and the polarization index (the difference between vertical and horizontal components of brightness temperature divided by their sum), were computed using the database developed in the current investigation. Average values of these three indices for the three intensive sampling areas were extracted and correlated with volumetric soil moisture. Table 3 shows the results of the coefficient of determination for these three vegetation indices. The normalized temperature difference between 37 GHz V and 37 GHz H has the highest coefficient of determination for all three sampling areas. However, the value of the coefficient of determination decreases from CF to LW as vegetation density increases among these three sampling areas. The other two vegetation indices show the same trend but with smaller values of the coefficient of determination . Based upon this result, the normalized temperature difference between 37 GHz V and 37 GHz H was incorporated into the retrieval algorithm to estimate the optical depth. However, the results indicate that this parameter overestimates the effects of vegetation.

Following Jackson (1997), the average values of the observed emissivity for the three intensive sampling sites were extracted from the databases and were plotted against the observed volumetric soil moisture values (Figure 6). The theoretical model used to compute the predicted values of the observed emissivity as a function of volumetric soil

moisture in Figure 3 was used to compute the observed emissivity values for the three intensive sampling areas with various optical depth values. As shown in Figure 6, for the CF most observations fall between the lines computed with optical depth equal to 0.4 and 0.5, for the LW between 0.6 and 0.7, and for the ER, between 0.55 and 0.65. Figure 7 shows the relationship between NDVI and the observed emissivity for the three areas during the entire experiment period. It indicates that each intensive sampling area had a consistent vegetation condition since the NDVI values for each area form a cluster. Thus, for this study, the b parameter is an average value for each cluster such that the product of this value and the NDVI value of a pixel in a specific area will be between the two predicted lines shown in Figure 6 for each intensive sampling area. Pixels outside the intensive sampling areas with an NDVI value in the range of one of the intensive sampling areas will be assigned the same b value as that area. However, when a pixel has a higher NDVI value than the highest value in the LW, its optical depth was assigned to the highest value of the LW.

5.3. Discussion

If one assumes that vegetation condition, or the NDVI, does not change rapidly from day to day, then the difference in emissivity from day to day can be attributed to the increase/decrease of soil moisture due to rainfall/evapotranspiration. Figure 7 describes the changes in normalized brightness temperature of the three intensive sampling areas for the SSM/I data selected for this study. This figure clearly shows that, as expected, the CF has the lowest NDVI values and the largest changes in the observed emissivity. On the other hand, the LW has the highest NDVI values with the smallest changes in the observed emissivity.

Figure 8a indicates that when there was some rainfall over the CF area on June 26, the emissivity dropped from approximately 0.935 on June 25 to approximately 0.866 on June 27. The increase of about 20% of soil moisture from June 25 to June 26 over the CF area (Table 2) corresponds to a decrease of about 7% of emssivity. The sensitivity to soil moisture is much less than at L-band (Figure 3). Although NDVI increases from late June to early July, a similar sensitivity to increased soil moisture can be observed over the CF area, with approximately a 20% change in soil moisture corresponding to about a 10% change in the observed emissivity (Figure 7a). However, a similar 20% change in volumetric soil moisture occurred over the LW and the ER area (Table 2) during the experiment period and only produced a 3 - 4% change in the observed emissivity at these two areas (Figure 8b and 8c).

According to Figure 8, there were a number of rainy days during SGP97. It was necessary to check if the SSM/I data were contaminated by ongoing rain before the retrieval algorithm was applied to them. The parameter developed by Grody (1991) was used to screen SSM/I pixels for contamination. This parameter is defined as:

$$SIL = 451.9 - 0.44TB_{19V} - 1.775TB_{22V} + 0.00575TB_{22V}^{\ 2} - TB_{85V} \qquad (12)$$

When SIL is greater than 10 K, it indicates that the SSM/I 19 GHz pixel probably had ongoing rain. These contaminated pixels were masked out. The mask images show that rainfall occurred outside the SGP region during the satellite overpass for those orbits selected for this study.

A difference in the approach used here as opposed to Jackson (1997) was that the volumetric soil moisture of every pixel in the SSM/I 19 GHz H polarization images was estimated using the physically based retrieval algorithm. The soil moisture images

derived by applying the retrieval algorithm to the SSM/I data are shown in Figure 9 along with the corresponding soil moisture image derived from the ESTAR data. As expected from the difference in the original resolution, the soil moisture images derived from the SSM/I data represent the regional wet/dry pattern. However, local details observed in the ESTAR results were lost. On June 25, both SSM/I and ESTAR soil moisture images show a dry condition. After the rainfall on June 26 over the northern two-thirds of the experiment region, the SSM/I data responded to the increase in soil moisture as shown in the June 27 moisture image (Figure 9). The SSM/I soil moisture image of June 30 indicates a drier condition than estimated from ESTAR. This difference may be physically based since the SSM/I signal is only representative of the top few millimeters of the surface while ESTAR responds to the top 5 cm or more. On July 1 and 2, the SSM/I soil moisture images again show the overall wet/dry pattern after the heavy rainfall on June 30. However, details of the soil moisture condition over the most northern portion are completely lost in the July 2 SSM/I soil moisture image. The July 3 images also show a drydown process. After raining in the northern part of the experiment region on July 11, the images from July 12, 13 and 16 describe a drying process, except for the most northern portion area in SSM/I moisture images.

The loss of local detail from ESTAR to SSMI can be attributed both to SSM/I's greater sensitivity to vegetation and to its larger footprint compared to ESTAR. Although the SSM/I data were interpolated to 800 m, the original satellite observation is the average of a 69 km by 43 km area. The difficulty in correcting for vegetation effects on SSM/I 19 GHz data is clearly shown over the northern panhandle area. A false color TM image taken on July 25, 1997 of this region indicated dense vegetation (Jackson et al., 1999).

Since the b related parameter was truncated at the LW NDVI level, this parameter may underestimate the effect of vegetation and overestimate the volumetric soil moisture in this particular area.

The contributing depth of soil to the measurement between 1.4 GHz and 19 GHz is also different. This fact may be the source of some differences in moisture level between the images derived from these two microwave sensors. The ground soil moisture sampling depth of 0-5 cm was designed for comparison with the ESTAR data. This set of 0-5 cm data was also used to evaluate soil moisture retrieval with the SSM/I observations even though the contributing soil depth is much shallower.

The average estimated soil moisture values for the three intensive sampling areas were extracted from the soil moisture images derived from SSM/I data and compared to the ground observations. The root mean square error (RMSE) for these three areas over 10 days is 7.81% (Figure 10) as contrasted to an RMSE of 2.82% for the same study areas over the same time period using ESTAR data (Jackson et al., 1999). However, the root mean square error differed among the sampling areas. If one examines the estimated and measured soil moisture over the LW, the SSM/I RMSE is 3.97% which is rather close to the overall results from the ESTAR data. Larger errors were found for the CF and the ER areas. The difficulty in estimating soil moisture for ER can be explained by the ungrazed grassland which has lower NDVI value and higher water content as compared to the LW. Since the NDVI values represented the composite for a half month period, for a wheat stubble dominated area such as CF these values may not indicate the true daily surface condition.

6. Conclusions

Previous studies by Pampaloni and Paloscia (1986) and Paloscia and Pampaloni (1988) suggest that microwave data with frequencies higher than 10 GHz are not appropriate for soil moisture estimation since the vegetation will strongly mask out surface information. However, in their recent study, Calvet et al. (1995b) indicated that the top surface soil moisture can be retrieved with acceptable accuracy at higher microwave frequencies if dense patchy vegetation coverage is below 50% of the area or sparse vegetation such as agricultural crops at their early stage of growth. The current study similarly showed that under certain conditions SSM/I data can be used to retrieve surface soil moisture information at a regional scale. Vegetation parameters derived from satellite observations such as NDVI from AVHRR and a theoretical model can provide adequate information to estimate the vegetation optical depth which can then be incorporated in the soil moisture retrieval algorithm. The results of applying this physically based soil moisture retrieval algorithm to SSM/I data taken during the SGP97 produced an estimated error in volumetric soil moisture of 7.81% over three intensive sampling areas with different vegetation regimes. The estimated error can be improved over some sparsely vegetated surfaces if more frequent NDVI values can be obtained. Surface soil moisture can not be retrieved when there is heavy vegetation using 19 GHz measurements. If accurate estimation of surface soil moisture is required for other applications, such as global climate modeling, then an L band spaceborne radiometer system would be more suitable for the work. This study also indicates that the empirical approach developed by Choudhury (1993) can be used to correct the effect of the atmosphere for SSM/I data when radiosonde data are not available.

Acknowledgement

The authors would like to thank those individuals who participated the Southern Great Plains 1997 Hydrology Experiment. Collecting the data necessary for SGP97 was only possible because of exceptional efforts of the soil moisture sampling teams that went out every day and the NASA Wallops Flight Facility P3B aircraft team that made the ESTAR mission possible. They would also like to thank the Atmospheric Radiation Measurement (ARM) Program sponsored by the US Department of Energy for providing radiosonde data and the GIMMS group, NASA/GSFC for providing NDVI data derived from AVHRR. Finally, they also wish to thank Dr. M. Y. Wei of NASA Headquarters whose guidance and support made this project of greater value than its individual components.

References:

Calvet, J.-C., J.-P. Wigneron, A. Chanzy, S. Raju, and L. Laguerre, "Microwave dielectric properties of a silt-Loam at high frequencies," ," IEEE Trans. on Geoscience and Remote Sensing, vol. 33, pp. 634-642, 1995a.

Calvet, J.-C., J.-P. Wigneron, A. Chanzy, and D. Haboudane, "Retrieval of surface parameters from microwave radiometry over open canopies at high frequencies," Remote Sens. Environ., vol. 53, pp. 46-60, 1995b.

Choudhury, B. J., T. J. Schmugge, and T. Mo, "A parameterization of effective temperature for microwave emission," J. Geophys. Res., vol. 87, pp. 1301-1304, 1982.

Choudhury, B. J., "Reflectivities of selected land surface types at 19 and 37 GHZ from SSM/I observations,' Remote Sens. Environ., vol. 46, pp. 1-17, 1993.

Ferrazzoli, P., L. Guerriero, S. Paloscia, P. Pampaloni, and D. Solimini, "Modeling polarization properties of emission from soil covered with vegetation," IEEE Trans. on Geoscience and Remote Sensing, vol. 30, pp157-165, 1992.

Grody, N. C., "Classification of snowcover and precipitation using the special sensor microwave imager," J. Geophys. Res., vol. 96,pp. 7423-7435, 1991.

Hallikainen, M. T., F. T. Ulaby, M. C. Dobson, M. A. El-Rayes, and L. K. Wu, "Microwave dielectric behavior of wet soil – Part I: Empirical models and experimental observations," IEEE Trans. on Geoscience and Remote Sensing, vol. GE-23, pp. 25-34, 1985.

Heymsfield, G. A., and R. Fulton, "Modulation of SSM/I microwave soil radiances by rainfall," Remote Sens. Environ., vol. 29, pp. 187-202,1992.

Hollinger, J. P., J. L. Peirce, and G. A. Poe, "SSM/I instrument evaluation," IEEE Trans. on Geoscience and Remote Sensing, vol. 28, pp. 781-790, 1990.

Hollinger, S. E., and C. S. T. Daughtry, "Southern Great Plains 1997 Hydrological Experiment: Vegetation sampling and data documentation," report to USDA/ARS on contract AG 58 1270 7 043, pp. 52, May, 1999.

Jackson, T. J., T. J. Schmugge, and J. R. Wang, "Passive microwave sensing of soil moisture under vegetation canopies," Water Resources Research, vol. 18, pp. 1137-1142, August, 1982.

Jackson, T. J., and T. J. Schmugge, "Vegetation effects on the microwave emission of soil," Remote Sens. Environ., vol. 36, pp.203-212, 1991.

Jackson, T. J., "Measuring surface soil moisture using passive microwave remote sensing," Hydrol. Process., vol. 7, pp. 139-152, 1993.

Jackson, T. J., D. M. Le Vine, C. T. Swift, T. J. Schmugge, and F. R. Schiebe, "Large area mapping of soil moisture using the ESTAR passive microwave radiometer in Washita '92," Remote Sens. Environ., vol. 54, pp. 27-37, 1995.

Jackson, T. J., "Soil moisture estimation using special satellite microwave/imager satellite data over a grassland region," Water Resources Research, vol. 33, pp.1475-1484, June 1997.

Jackson, T. J, D. M. Le Vine, A. Y. Hsu, A. Oldak, P. J. Starks, C. T. Swift, J. D. Isham, and M. Haken, "Soil moisture mapping at regional scales using microwave radiometry: The Southern Great Plains Hydrology Experiment,' IEEE Trans. on Geoscience and Remote Sensing, vol. 37, pp. 2136-2151, 1999.

Kirdiashev, K. P., A. A. Chukhlantsev, and A. M. Shutko, "Microwave radiation of the Earth's surface in the presence of vegetation cover," Radio Eng. Electron. Phys., Vol. 24, pp. 256-264, 1979 (Engl. Transl.).

Le Vine, D. M., A. J. Griffis, C. T. Swift, and T. J. Jackson, "ESTAR: a synthetic aperture microwave radiometer for remote sensing application," Proc. Of the IEEE, vol. 82, pp. 1787-1801, 1994.

Meeks, M. L., and A. E. Lilley, "The microwave spectrum of oxygen in the Earth's atmosphere," J. Geophys. Res., vol. 68, pp.1683-1703, 1963.

Paloscia, S., and P. Pampaloni, "Microwave remote sensing of plant water stress," Remote Sens. Environ, vol. 16, pp. 249-255, 1984.

Paloscia, S., and P. Pampaloni, "Microwave vegetation indexes for detecting biomass and water conditions of agricultural crops, Remote Sens. Environ, vol. 40, pp. 15-26, 1992.

Pampaloni, P., and S. Paloscia, "Microwave emission and plant water content: A comparison between field measurements and theory," IEEE Trans. on Geoscience and Remote Sensing, vol. GE-24, pp. 900-905, 1986.

Ulaby, F. T., R. K. Morre and A. K. Fung, Microwave Remote Sensing: Active and Passive, Vol. 1, Reading, MA: Addison-Wesley, 1981.

Ulaby, F. T., M. Razani, and M. C. Dobson, "Effects of vegetation cover on the microwave radiometric snesitivity of soil moisture," IEEE Trans. on Geoscience and Remote Sensing, vol. GE-21, pp. 51-61, 1983.

Wang, J. R., and T. J. Schmugge, "An empirical model for the complex dielectric permittivity of soils as a function of water content," IEEE Trans. on Geoscience and Remote Sensing, vol. GE-18, 288-295, 1980.

List of Figures

1. Map of SGP97 area and related networks for environmental monitoring

2. Brightness temperatures measured by the ESTAR at 1.4 GHz H and the SSM/I at 19 GHz H on July 2, 1997

3. Emissivity comparison of 1.4 GHz H and 19 GHz H

4. NDVI images of the Central U.S. generated by GIMMS for late June and early July, 1997

5. Schematic diagram of soil moisture retrieval algorithm

6. Volmetric soil moisture as a function of emissivity at 19 GHz H for the three intensive sampling sites

7. Relationship between normalized brightness temperature at 19 GHz H and NDVI during the SGP97: (a) CF, (b) LW, and (c) ER

8. Relationship between rainfall and observed emissivity during the SGP97: (a) CF, (b) LW, and (c) ER

9. Comparison of retrieved soil moisture between ESTAR and SSM/I

10. Comparison of estimated and ground measured soil moisture

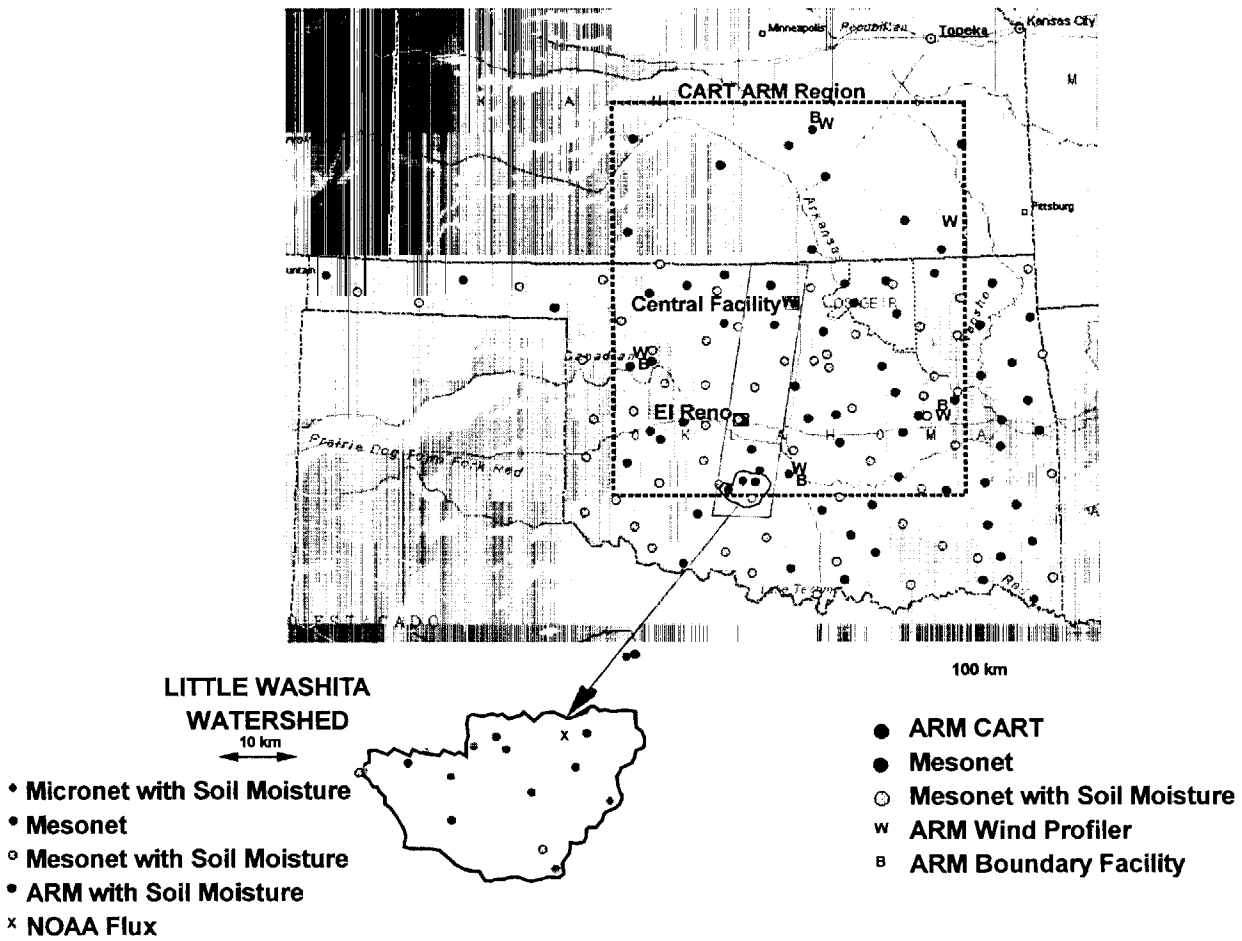
CART ARM Region
Central Facility
El Reno
Topeka
Kansas City
Minneapolis
Pittsburg
100 km
LITTLE WASHITA
WATERSHED
10 km
• Micronet with Soil Moisture
• Mesonet
○ Mesonet with Soil Moisture
• ARM with Soil Moisture
x NOAA Flux
● ARM CART
● Mesonet
○ Mesonet with Soil Moisture
W ARM Wind Profiler
B ARM Boundary Facility

Figure 1

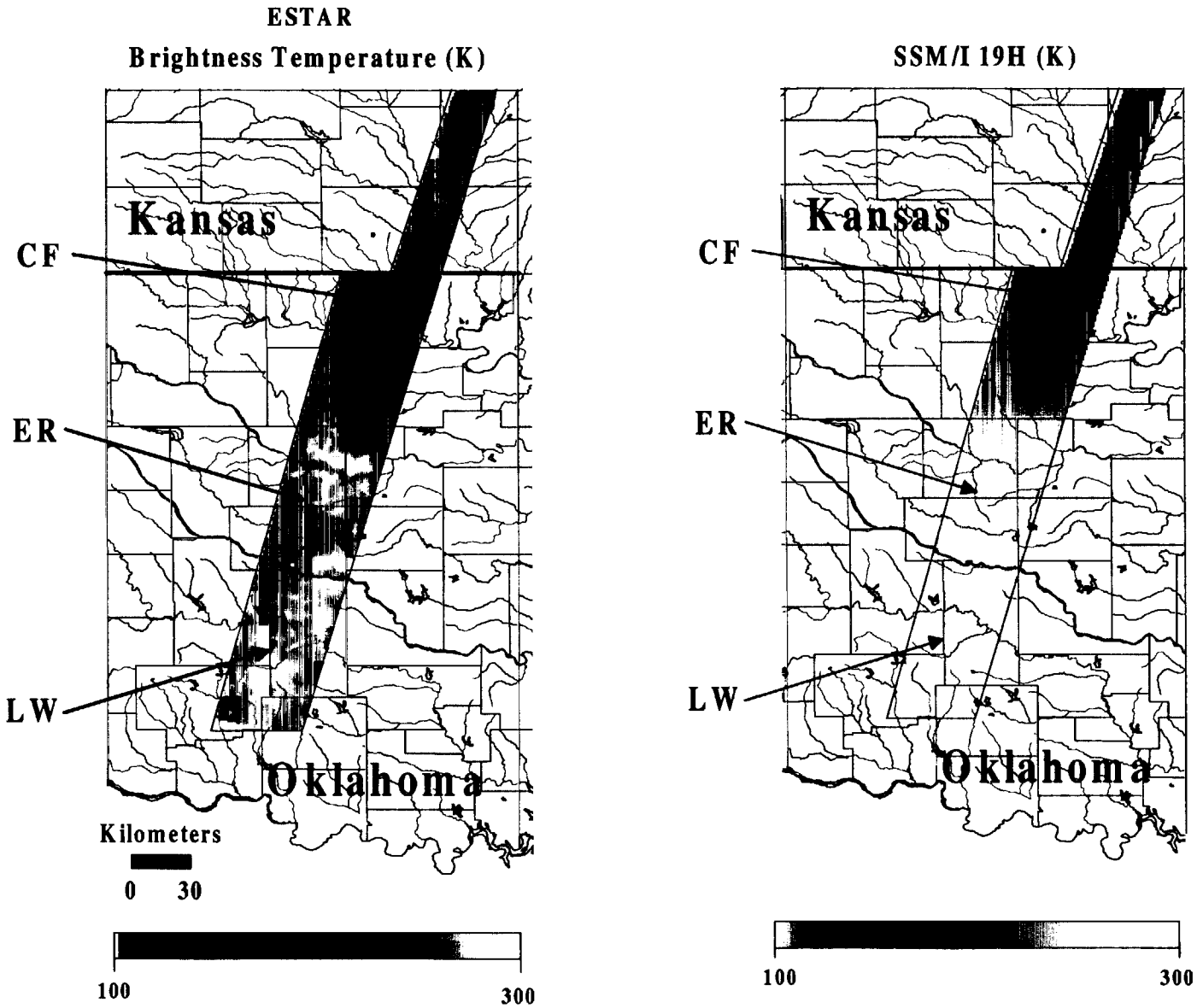
ESTAR
Brightness Temperature (K)
Kansas
CF
ER
LW
Oklahoma
Kilometers
0 30
100
300
SSM/I 19H (K)
Kansas
CF
ER
LW
Oklahoma
100
300

Figure 2

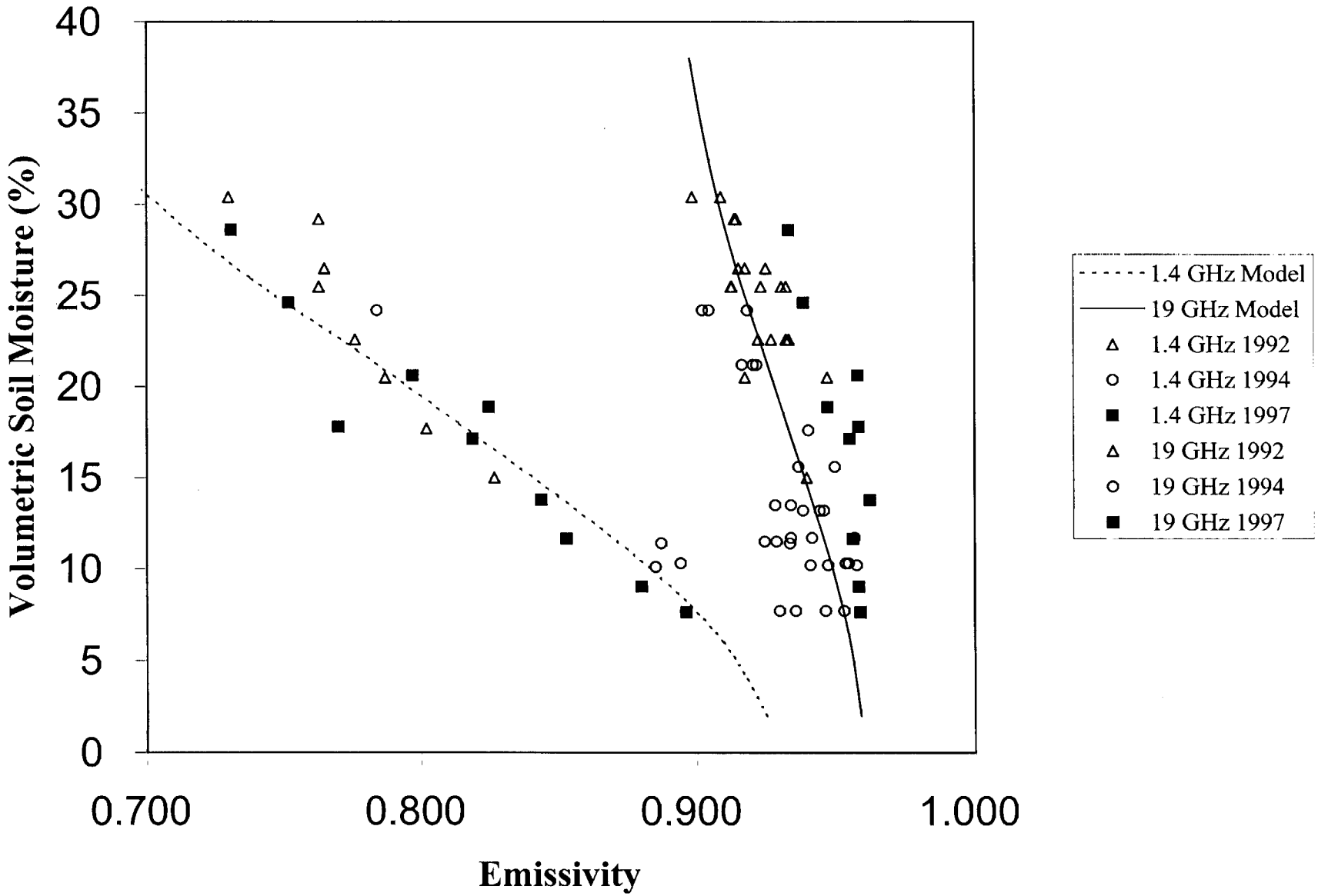
Volumetric Soil Moisture (%)
40
35
30
25
20
15
10
5
0
0.700
0.800
0.900
1.000
Emissivity
1.4 GHz Model
19 GHz Model
1.4 GHz 1992
1.4 GHz 1994
1.4 GHz 1997
19 GHz 1992
19 GHz 1994
19 GHz 1997

Figure 3

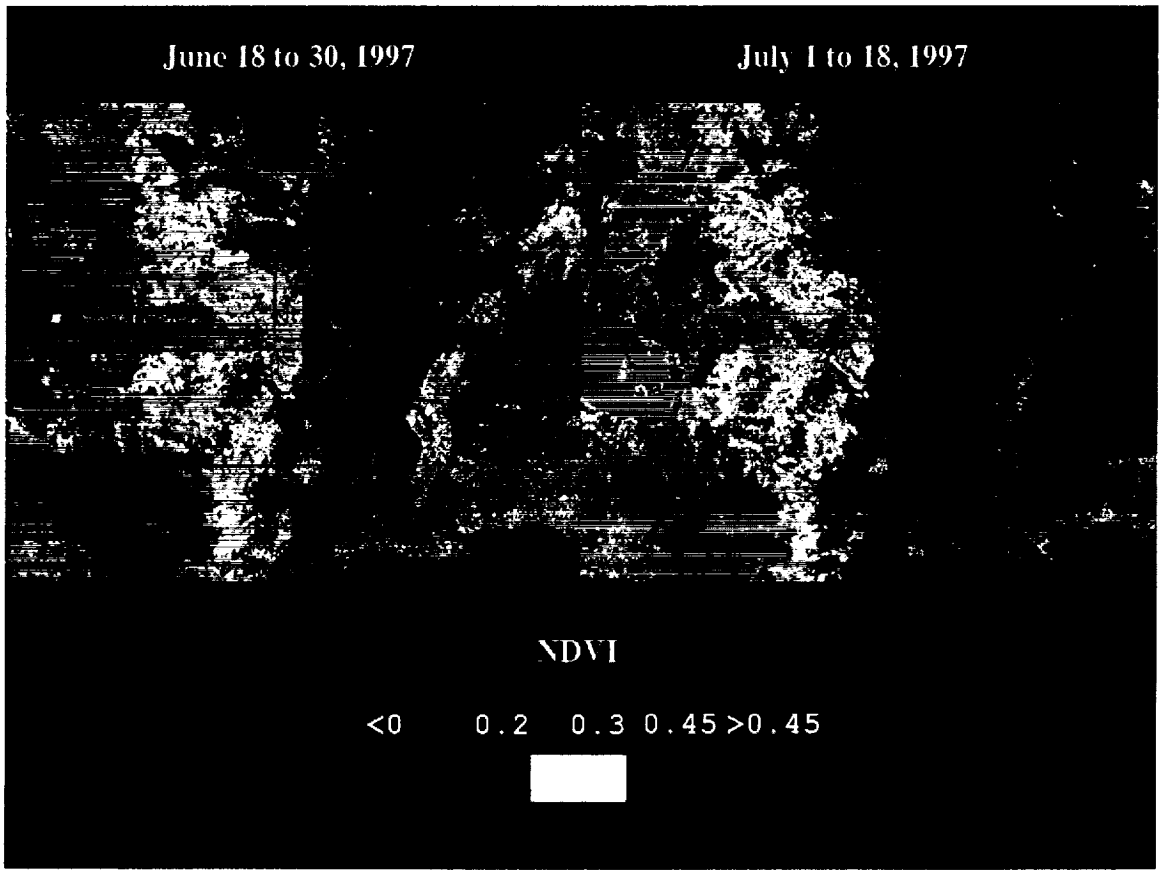

Figure 4

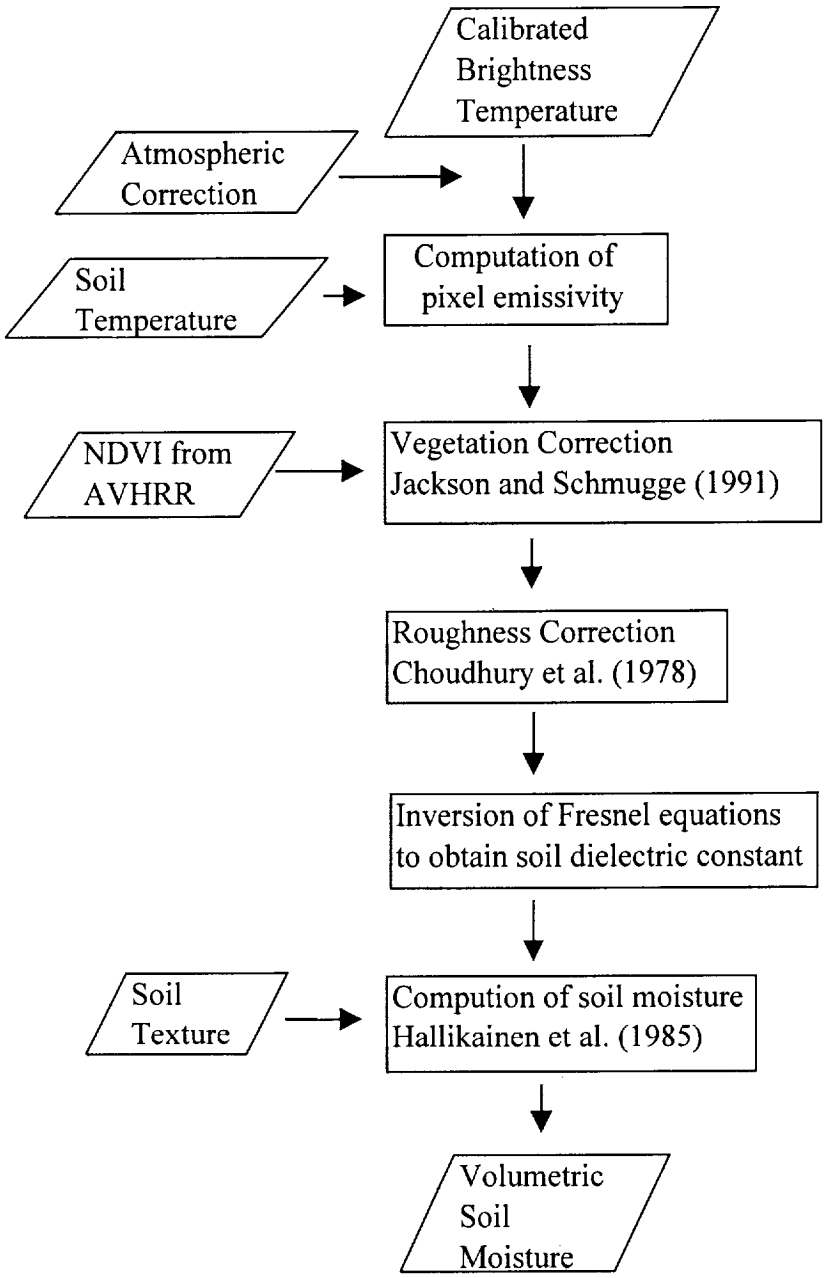
Calibrated Brightness Temperature
Atmospheric Correction
Soil Temperature
Computation of pixel emissivity
NDVI from AVHRR
Vegetation Correction Jackson and Schmugge (1991)
Roughness Correction Choudhury et al. (1978)
Inversion of Fresnel equations to obtain soil dielectric constant
Soil Texture
Compution of soil moisture Hallikainen et al. (1985)
Volumetric Soil Moisture

Figure 5

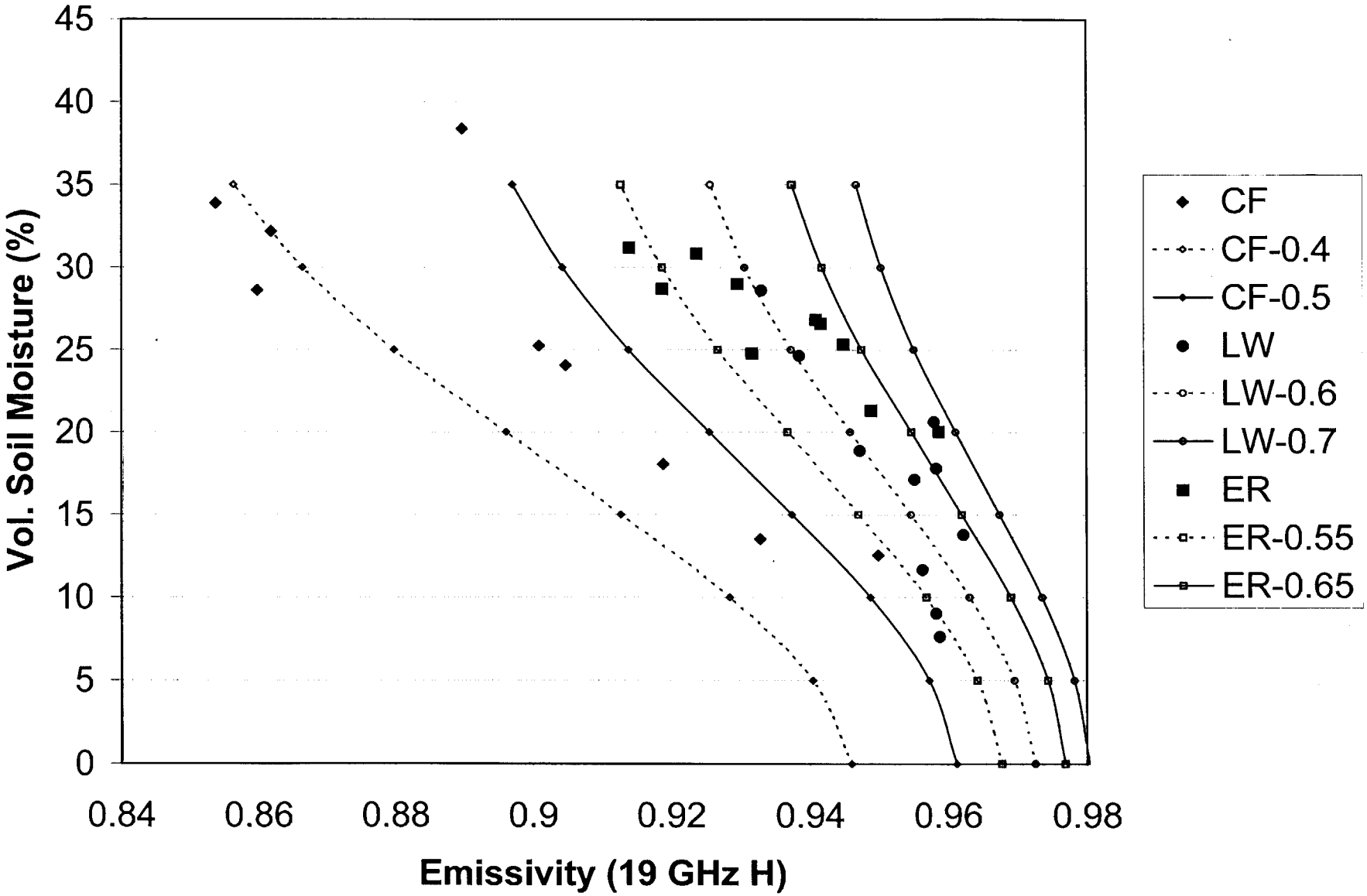
Vol. Soil Moisture (%)
45
40
35
30
25
20
15
10
5
0
0.84
0.86
0.88
0.9
0.92
0.94
0.96
0.98
Emissivity (19 GHz H)
CF
CF-0.4
CF-0.5
LW
LW-0.6
LW-0.7
ER
ER-0.55
ER-0.65

Figure 6

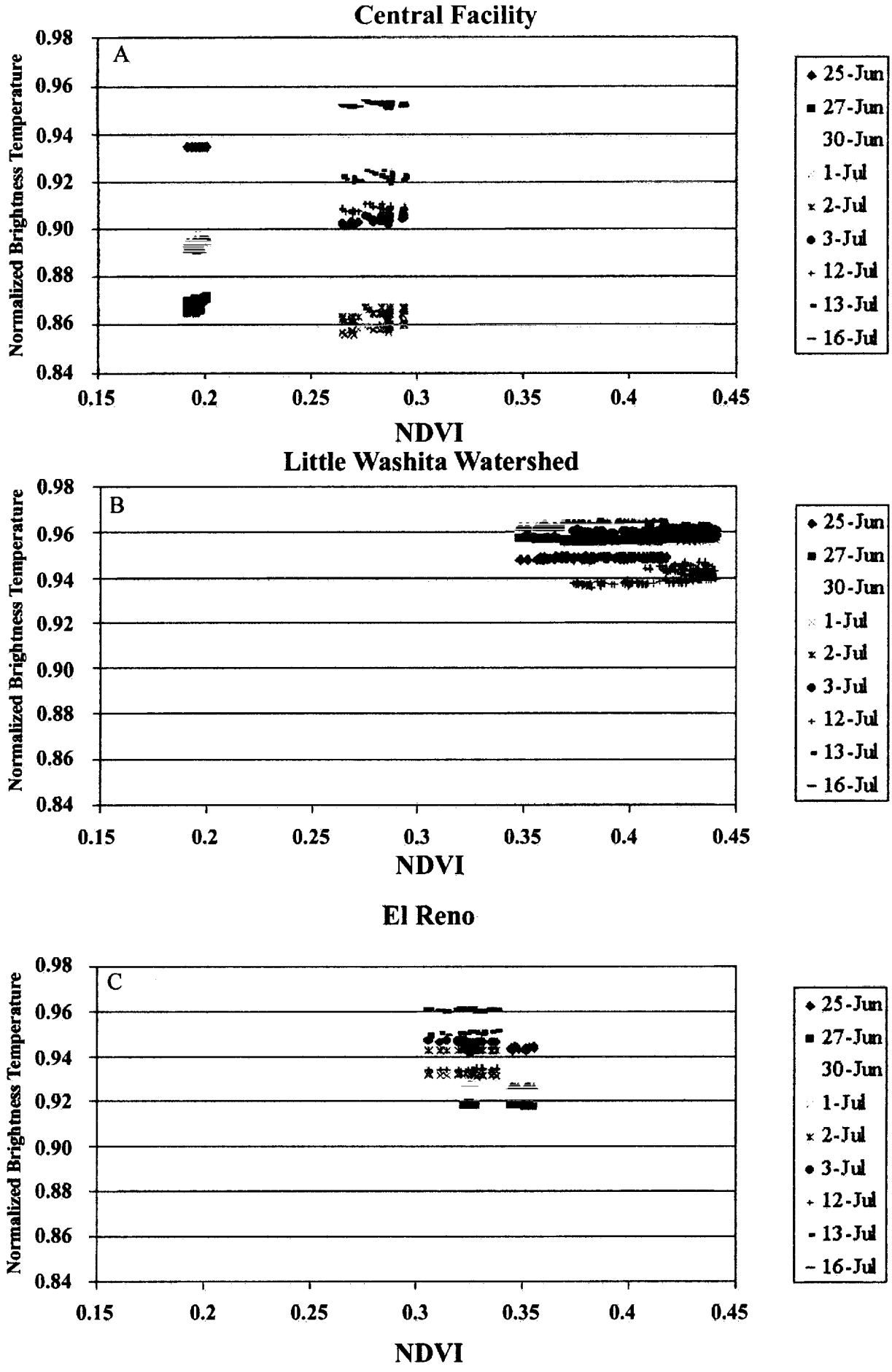
Central Facility
A
Normalized Brightness Temperature
0.98
0.96
0.94
0.92
0.90
0.88
0.86
0.84
0.15
0.2
0.25
0.3
0.35
0.4
0.45
NDVI
25-Jun
27-Jun
30-Jun
1-Jul
2-Jul
3-Jul
12-Jul
13-Jul
16-Jul
Little Washita Watershed
B
Normalized Brightness Temperature
NDVI
El Reno
C
Normalized Brightness Temperature
NDVI

Figure 7

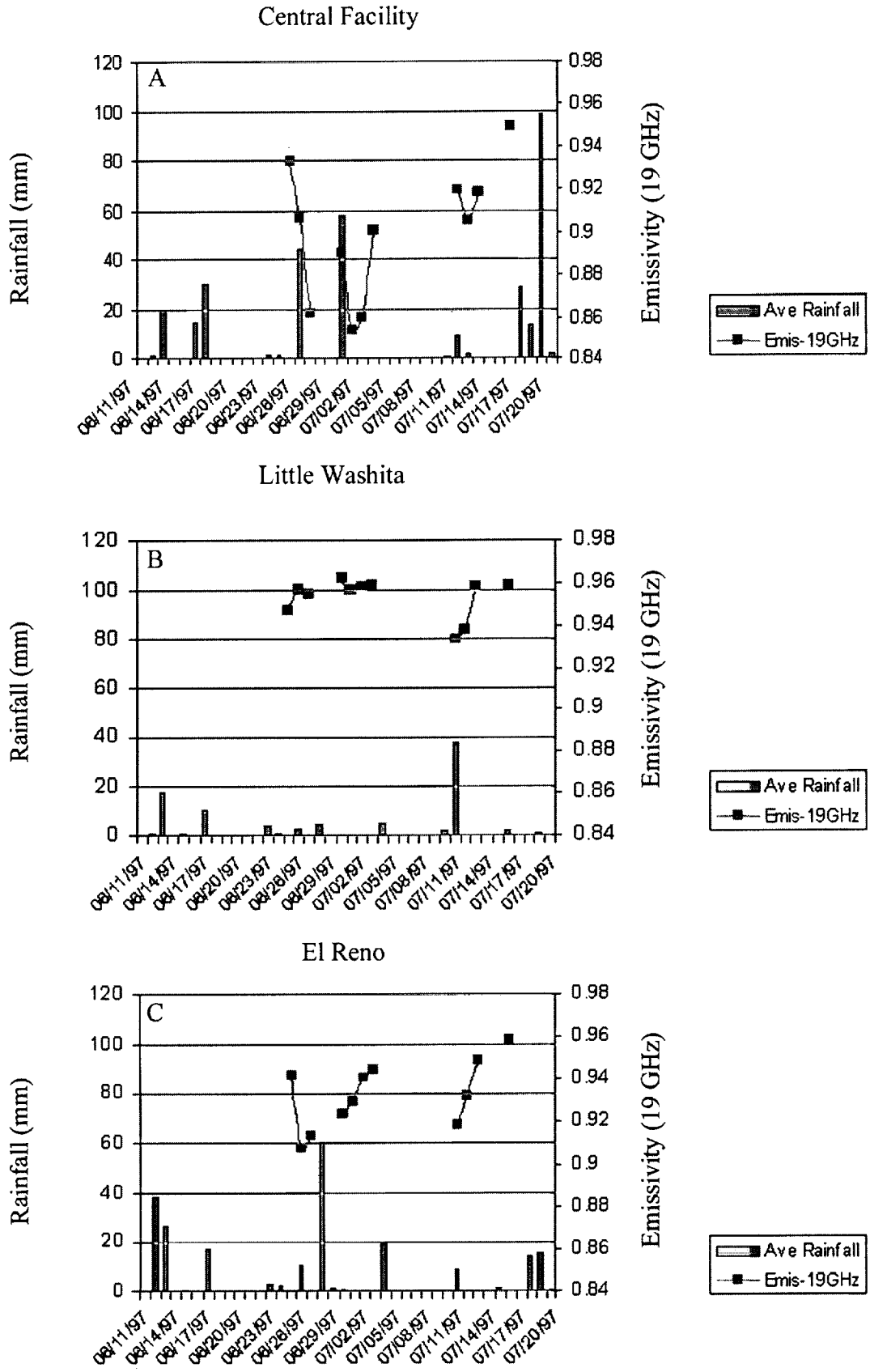
Central Facility
A
Rainfall (mm)
Emissivity (19 GHz)
120
100
80
60
40
20
0
0.98
0.96
0.94
0.92
0.9
0.88
0.86
0.84
Ave Rainfall
Emis-19GHz
08/11/97
08/14/97
08/17/97
08/20/97
08/23/97
08/26/97
08/29/97
07/02/97
07/05/97
07/08/97
07/11/97
07/14/97
07/17/97
07/20/97
Little Washita
B
Rainfall (mm)
Emissivity (19 GHz)
Ave Rainfall
Emis-19GHz
El Reno
C
Rainfall (mm)
Emissivity (19 GHz)
Ave Rainfall
Emis-19GHz

Figure 8

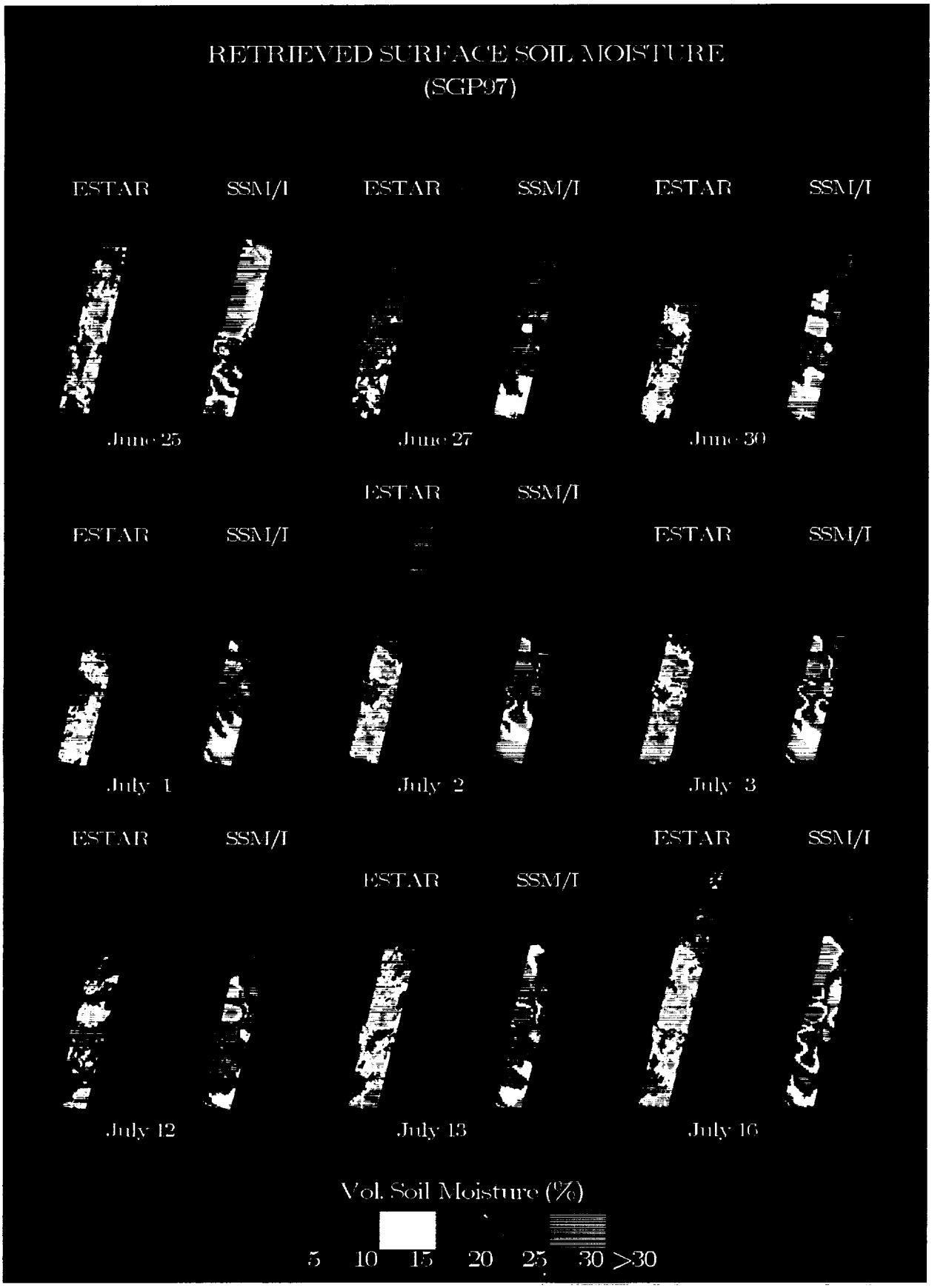
RETRIEVED SURFACE SOIL MOISTURE
(SGP97)
ESTAR
SSM/I
ESTAR
SSM/I
ESTAR
SSM/I
June 25
June 27
June 30
ESTAR
SSM/I
ESTAR
SSM/I
ESTAR
SSM/I
July 1
July 2
July 3
ESTAR
SSM/I
ESTAR
SSM/I
ESTAR
SSM/I
July 12
July 13
July 16
Vol. Soil Moisture (%)
5
10
15
20
25
30
>30

Figure 9

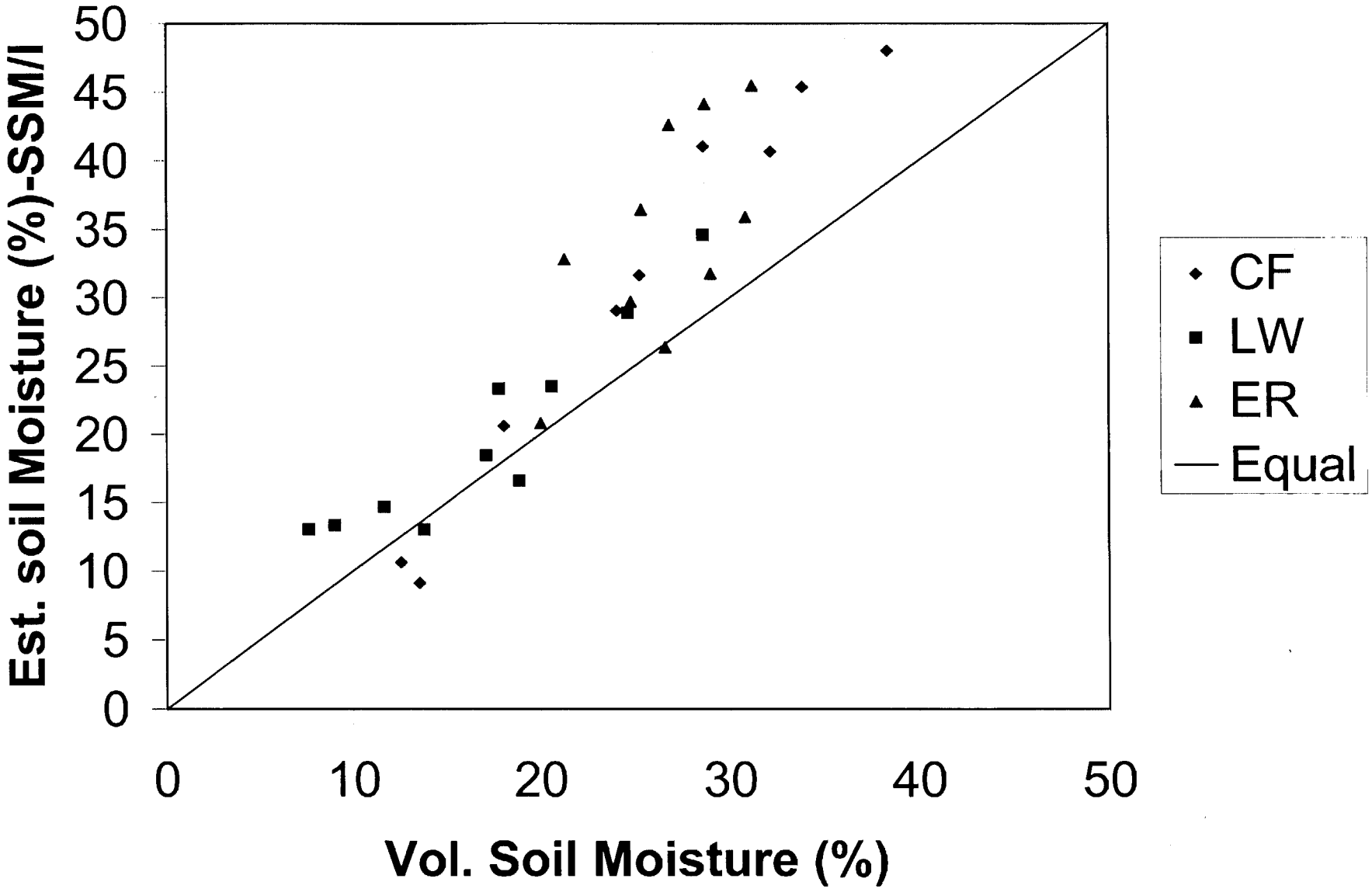
Est. soil Moisture (%)-SSM/I
50
45
40
35
30
25
20
15
10
5
0
0
10
20
30
40
50
Vol. Soil Moisture (%)
CF
LW
ER
Equal

Figure 10